TJES
ISSN: 1813-162X
Tikrit Journal of Engineering Sciences
available online at: http://www.tj-es.com

Performance Prediction of Internal Compression Supersonic Air Intake at Range of Mach Numbers (1.1-1.5)

Hasson Shaban Hamood
Technical College-Mosul, Iraq

Abstract

In this research a numerical investigation on a supersonic air intake was done. The aim of this work is to investigate a variable geometry of cross-section area for supersonic air intake at range (1.1-1.5) Mach number, to get a maximum pressure recovery. In this work, the flow starts with a normal shock attached to the intake cowl lip. The flow is assumed compressible, inviscid, two-dimensional flow, unsteady, and axisymmetric. The equations (Continuity, Momentum, and Energy) were solved based on a finite volume method. The governing equations were solved iteratively using time marching technique. This part is analyzed for several Mach numbers, where the flow properties are determined from inlet of air intake to the diffuser exit. Results show that, the implementation of time marching scheme has succeeded in the prediction of the choked flow region, which is important in the study of the performance of convergent-divergent diffuser. Also the results indicated the absolute velocity increases along the convergent part and then start to decrease along divergent part independently on the values of free-stream Mach numbers.

Keywords: Convergent-divergent diffuser, Supersonic air intake, Finite volume method, Time marching techniques.

التنبؤ بأداء آخذة هواء فوق صوتية تعمل بمبدأ الانضغاط الداخلي لأرقام ماخ (1.1-1.5)

الخلاصة

تم في هذا البحث التنبؤ العددي لأداء آخذة هواء فوق صوتية. الغرض من هذا البحث فحص آخذة هواء فوق صوتية متغيرة في مقطع المساحة لأرقام ماخ تتراوح ما بين (1.1-1.5) للحصول على أعلى ضغط إرجاعي. في هذا العمل، يبدأ عمل الآخذة بموجة صدمة عمودية عند مدخل الآخذة وبالتالي فان الجريان ما بعد الصدمة العمودية هو جريان دون صوتي على طول الناشر الملتم. تم فرض الجريان على انه جريان غير لزج، ثنائي البعد، غير مستقر، ومتناسق مع المحور.استخدمت الطريقة العددية لحل معدلات (الاستمرارية، الزخم، والطاقة) معتمدا على طريقة الحجم المحدد. تم حل المعادلات السابقة حلا تكراريا باستخدام آلية الزحف الزمني. تم تحليل هذا الجزء لعدة قيم ماخ من مدخل الآخذة (النشر الملتم) وحتى مخرج الناشر. بينت نتائج البحث بان طريقة الزحف الزمني كانت موفقة في التنبؤ بموقع اختناق الجريان، كما بينت النتائج السلوك الطبيعي للجريان دون الصوتي ما بعد الموجة العمودية على طول النشر الملتم-المنفرج. كذلك أشارات النتائج إلى زيادة قيمة السرعة المطلقة على طول الجزء الملتم بينما تبدأ بالنقصان على طول الجزء المنفرج غير معتمدة على قيم رقم ماخ الجريان الحر.

الكلمات الدالة: الناشر الملتم- المنفرج، آخذة الهواء فوق الصوتية، طريقة الحجم المحدد، تقنية الزحف الزمني.

Nomenclature

Item	Symbol	Unit
Absolute velocity	c	m/s
Altitude	H	m
Area of cell in X-dir.	A_x	m^2
Area of cell in Y-dir.	A_y	m^2
Damping factor	B	---
Damping term	D	---
Diffuser height	d	m
Diffuser inlet section	c	---
Diffuser exit section	e	---
Downstream of Mach Number	y	---
Flux of mass	F(i,j)	---
Flux of momentum in X-dir.	$F(i,j)_x$	---
Flux of momentum in Y-dir.	$F(i,j)_y$	---
Flux vector-tension in X-dir.	f	---
Flux vector-tension in Y-dir.	g	---
Flux vector-tension in t-dir.	U	---
Length of diffuser	L	m
Mach Number	M	---
Node in X-dir.	i	---
Node in Y-dir.	j	---
Relaxation term	CF	---
Relaxation factor	RF	---
Speed of sound	a	m/s
Static pressure	P	N/m^2
Static temperature	T	K
Temporal index	n	---
Time	t	sec
Total energy per unit mass	E	J/kg
Velocity component in X-dir.	u	m/s
Velocity component in Y-dir.	v	m/s
Volume of cell	vol.	m^3
Upstream of Mach Number	x	---
Air density	ρ	kg/m^3
Specific heat ratio	γ	---
Diffuser exit divergence angle	θ	deg.
Diffuser inlet convergence angle	δ	deg.
Free stream Mach Number	∞	---

Introduction

The prediction of flow in air intake is of practical importance in the development and design of air intake. So a large number of studies has been done to analyze the characteristics of flow field. Some of these studies were concentrating on subsonic air intake. A large number of these studies were concentrating on supersonic air intake.

Conners et al.[1], presented design charts for Mach numbers up to 4, for single and double-oblique and conical-shock inlets and for isentropic axi-symmetric and two-dimensional surfaces having theoretically focused Mach lines. Compression limits for isentropic inlets are presented. A comparison of optimum performance for various inlet configurations (normal shock, convergent-divergent (internal compression), single cone, double cone, and isentropic) is presented. The geometric angles of the single and double cone inlets were optimized in terms of pressure recovery by using Taylor-Maccoll method.

Knight et al.[2], developed a numerical code to calculate the flow field in two-dimensional high-speed inlets using the Navier-Stokes equations. The code has been applied to calculate the flow in a simulated high-speed inlet operating at a Mach number 2.5 and Reynolds number of 1.4×10^7 based on the inlet length. The computed results are compared with detailed measurements of the ramp and cowl static pressure. The agreement with the experimental data is good.

Shimabukuro et al.[3], conducted an analytical study on various inlet-engine combinations for a Mach 2.2, to select a preferred inlet type for single-engine pod installations. These types of inlets include two-dimensional and axisymmetric with either mixed or internal compression. The results of the study indicated that the axisymmetric mixed compression inlet was preferred. Detailed design studies of single and double cone axisymmetric mixed compression inlets types are discussed.

Biringen et al.[4], outlined a time-dependent, implicit, finite-volume solution procedure for the Euler equations, to calculate two-dimensional inlet flow fields. This work focuses on the calculation of inviscid inlet flow fields with uniform and non-uniform inflow boundary condition. All the calculations were performed at the design Mach number of the inlet 3.5. Results for a practical inlet configuration are presented. The method can be used for a flow field with both subsonic and supersonic regions and is found to converge rapidly for supercritical and sub critical inlet operations.

Walters et al.[5], presented a numerical method for solving the compressible Navier-Stokes equations in conservative form. This method was tested on a number of numerical

examples, one of them was a supersonic inlet. The supersonic inlet results were presented for 5˚ wedge inlet at free stream Mach number equal to 3. The results were in a good agreement with these of other methods, and/or experiments.

Moretti et al.[6], presented an efficient Euler computational technique for two-dimensional Euler equations at any number of shock of any shape and type, whose interaction can be treated by this technique. He presented the results for a number of examples, such as transonic airfoils, shock in ducts, intake flows, multiple Mach reflections. The results for intake were at free stream Mach number equal to 2, ended at outlet of duct of 0.3 Mach.

Mittal et al.[7], presented a numerical method to solve compressible Euler equations for two-dimension mixed compression supersonic inlet. A stabilized finite-element method is employed. The computations are capable of simulating the start-up problems associated with mixed compression supersonic inlets. If the diffuser throat is not large enough to allow the start-up normal shock wave to pass through the inlet it un starts.

The computation method is presented for design Mach number 3. The results were the start-up problem of inlet, which can be solved with either an increase of the throat area (variable geometry) or by increasing the free stream Mach number (fixed geometry).

In this work the supersonic air intake was investigated for a range of Mach numbers corresponding to ($M_\infty = 1.1-1.5$), and at specific altitude corresponding to ($H = 5000m$).

The operation of the air intake at low supersonic Mach number ($M_\infty \leq 1.5$) is considered as a normal shock intake, when the normal shock wave stands at the cowl lip of the intake[8]. The mechanism that locates the normal shock wave at this position is the variable throat area, which is opened further to permit the normal shock attachment to the cowl lips. In this case the flow is choked at throat position (M_t=1.0) as shown in Figure (1).

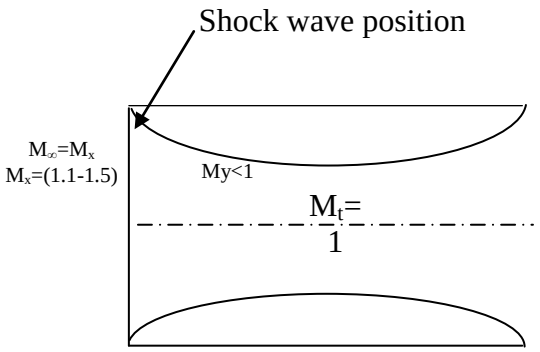

Fig. 1. Normal shock wave position during operation at low Mach numbers ($M_\infty \leq 1.5$)

Mathematical Model

The supersonic air intake, that shown in Figure (2), was considered as a variable cross-sectional area of intake with two internal facing ramps. This type of air intake achieves compression though using the variable throat area to allow the normal shock attached the cowl lip at every free stream Mach number[9].

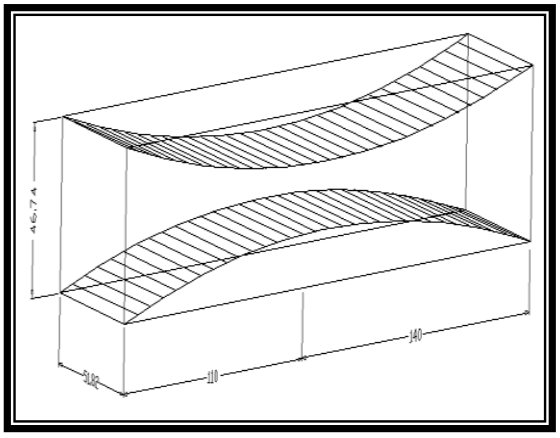

Fig. 2. Convergent-divergent supersonic diffuser configurations

The design elements of the convergent diffuser are (L_1, δ) as shown in Figure (3). Where the convergent length of this diffuser may be optimized in terms of total pressure recovery, where all pressure recoveries are based on shock losses. While the second part of diffuser consists of diverging passage starts immediately downstream of the converging part. The length of the divergent diffuser (L_2) is very important in design and it is optimized to

avoid flow separation. The design elements of divergent diffuser are (L_2,θ_e). These elements must be optimized to get intake with following characteristics, 1.Short enough to keep weights and drags to minimum, 2. Long enough to give Mach number range (0.2-0.5) at engine face[10].

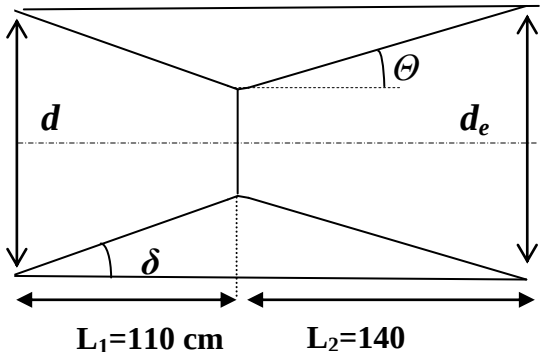

Fig. 3. Convergent-divergent supersonic diffuser design parameters

The flow requirement of an existing turbojet engine is used to determine the ranges of entrance to throat area (contraction ratio) variations that are employed in the mechanical design of the model. These area ratios and the shock configuration for optimum pressure recovery at the design point determine the length of the converging part. The length of the rear part is selected so that the maximum divergence angle at the design condition does not exceed (7^o), to avoid flow separation. This angle is considered to be a reasonable compromise between the requirements of minimum diffuser length and of maximum subsonic diffuser efficiency[11].

The performance of supersonic air intake has been predicted depending on design parameters that demonstrated at end of this paper. The air intake can be considered as a variable geometry convergent-divergent supersonic diffuser of two internal facing ramps. The compression that is happened at all free-stream Mach numbers will start with a normal shock wave attached to diffuser inlet cowl lips. The position of free stream Mach number in this case, is considered as attached to diffuser cowl lips, and it is equal to upstream Mach number (M_x), while the Mach number that located after the normal shock wave is equal to downstream Mach number (M_y). The time marching technique was used in this work to solve the flow equations along the whole diffuser (starting after a normal shock position with a subsonic Mach number) and continue until reach to diffuser end.

Assumptions

The following assumptions are made for the present work:-

1- The airflow was considered as a perfect gas.
2- The flow was considered as two-dimensional compressible along the whole diffuser.
3- Inviscid flow.
4- Unsteady flow.
5- Zero angle of attack.

Governing Equations

The mathematical behavior of the Euler partial differential equation is classified as elliptic in subsonic flow and hyperbolic in supersonic flow. If the time dependent terms are retained and a steady state is assumed as in current work the solution can be obtained using time marching procedure, by marching from some initial guessed flow field through time until a steady state is obtained, where all domains are expressed in hyperbolic differential equations. The governing equations for an inviscid, two-dimensional compressible flow expressed in a conservative form are[12]:

- Continuity equation

$$\frac{\partial(\rho)}{\partial t}+\frac{\partial(\rho u)}{\partial x}+\frac{\partial(\rho v)}{\partial y}=0 \quad \text{.....(1)}$$

- Momentum equations

In X-direction

$$\frac{\partial(\rho u)}{\partial t}+\frac{\partial(\rho u^2+P)}{\partial x}+\frac{\partial(\rho uv)}{\partial y}=0 \quad \text{.....(2)}$$

In Y-direction

$$\frac{\partial(\rho v)}{\partial t}+\frac{\partial(\rho vu)}{\partial x}+\frac{\partial\left(\rho v^2+P\right)}{\partial y}=0 \text{.....(3)}$$

- Energy equation

$$\frac{\partial(\rho E)}{\partial t}+\frac{\partial u(\rho E+P)}{\partial x}+\frac{\partial v(\rho E+P)}{\partial y}=0 \text{.....(4)}$$

where, E is given by the following equation:

$$E=\frac{P}{\gamma-1}+\frac{1}{2}\rho\times c^2 \text{.....(5)}$$

where, c is given by the following equation:

$$c=\sqrt{u^2+v^2} \text{ .....(6)}$$

It is convenient to combine the governing equations, into a compact vector before applying a finite volume algorithm to these equations. Euler Equations (1) through (4) in Cartesian coordinates may be written in a vector form[12]:

$$\frac{\partial U}{\partial t}+\frac{\partial f}{\partial x}+\frac{\partial g}{\partial y}=0 \text{ .....(7)}$$

The components *f* and *g* of the flux vector-tensor are defined in the following equations:

$$f=\begin{vmatrix}\rho u\\ \rho u^2+p\\ \rho uv\\ u(\rho E+P)\end{vmatrix} \text{.....(8)}$$

$$g=\begin{vmatrix}\rho v\\ \rho vu\\ \rho v^2+p\\ v(\rho E+P)\end{vmatrix} \text{.....(9)}$$

where, U is the proper vector which has the following components:

$$U=\begin{vmatrix}\rho\\ \rho u\\ \rho v\\ \rho E\end{vmatrix} \text{.....(10)}$$

By substituting Equations (8), (9), and (10) into Equation (7) it gives the following form:

$$\frac{\partial}{\partial t}\begin{vmatrix}\rho\\ \rho u\\ \rho v\\ \rho E\end{vmatrix}+\frac{\partial}{\partial x}\begin{vmatrix}\rho u\\ \rho u^2+p\\ \rho uv\\ u(\rho E+P)\end{vmatrix}+\frac{\partial}{\partial y}\begin{vmatrix}\rho v\\ \rho vu\\ \rho v^2+p\\ v(\rho E+P)\end{vmatrix}=0$$

.....(11)

Finite Volume Method

The complicated computational domains are often discratized without using transformation of the domain. From this point of view the method takes full advantage of an arbitrary mesh, where a large number of options are open for the definition of the control volumes around which the conservation laws are expressed. So the finite volume has the same flexibility as finite element methods. The time derivative was discratized to gives finally the following discredited system,

$$\vec{U}^{n+1}=\vec{U}^{n}+\frac{\Delta ti}{\Delta vol}\sum(\text{transport term})^{n}+\text{damping term} \text{ .....(12)}$$

where the transports term has to be taken as positive for transport into the element negative for a transport out of the element. The variables are stored at the center of the element and the Euler equations discratized on the finite volume in a conservation manner. The transport terms are computed at the cell faces assuming that they are linear between element centers.

Time Marching Techniques

The main attraction of the time marching method arises from its ability to handle mixed subsonic-supersonic flow with automatic inclusion of shock waves in a single calculation. This technique works naturally with a prescribed pressure ratio rather than with a prescribed mass flow, thereby avoiding the problem of finding the choking mass flow. This method is represented a solution of the time dependent Euler equations for different diffuser geometry by using a finite volume method with the time marching technique converging to the steady state. The new density and velocity associated with each (i,j) cell center, are determined from the continuity and momentum equations respectively by using the old values of density, velocities, and

pressure on the right hand side of the equations. The new pressure can be found from the constant enthalpy relationship (total temperature constant) using the new values of density and velocities as shown in the following procedure:

Continuity: $(\rho^n, u^n, v^n) \rightarrow \rho^{n+1}$ ……(13)

Momentum: $(\rho^n, u^n, v^n, P^n) \rightarrow u^{n+1}, v^{n+1}$ …..(14)

Energy: $(\rho^{n+1}, u^{n+1}, v^{n+1}) \rightarrow P^{n+1}$ ……(15)

Evaluation the Fluid Properties Using Finite Volume Method

The flow field is divided into a large number of arbitrary non-orthogonal finite element computational cells, as indicated in Figure (4).

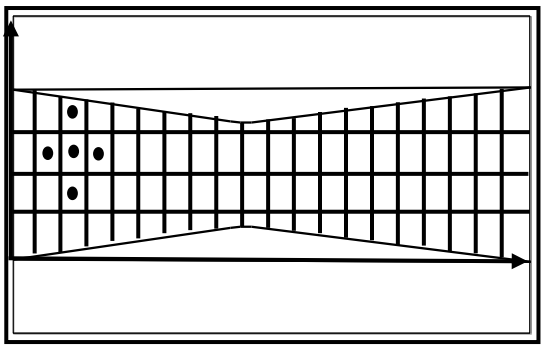

Fig. 4. Finite element technique with flow properties stored at center of cells

To solve the Euler equations, where the flow properties are stored at the centers of cells. The Euler equations can be written by using a summation of fluxes around the quadrilateral, and cell time differential can be written by a simple difference:

$$\frac{\Delta\rho}{\Delta ti}\cdot\Delta Vol=\sum_{cell.face}\left(\rho u\cdot\Delta Ax+\rho v\cdot\Delta Ay\right) \quad \text{……..(16)}$$

$$\frac{\Delta(\rho u)}{\Delta ti}\cdot\Delta Vol=\sum_{cell.face}\left(\left(\rho u^2+p\right)\cdot\Delta Ax+\rho uv\cdot\Delta Ay\right) \quad \text{……..(17)}$$

$$\frac{\Delta(\rho v)}{\Delta ti}\cdot\Delta Vol=\sum_{cell.face}\left(\rho uv\cdot\Delta Ax+\left(\rho v^2+p\right)\cdot\Delta Ay\right) \quad \text{……..(18)}$$

To compute the new values of the flow properties on the cell faces it is assumed that they change linearly between center of cells, so that the flux of mass into the (i,j)th cell across the face is:

(i,j) → (i+1,j+1) is:

$$F(i,j)=\frac{1}{2}\left[(\rho u)_{i,j}+(\rho u)_{i-1,j}\right]Ayy_{i,j}+\frac{1}{2}\left[(\rho v)_{i,j}+(\rho v)_{i-1,j}\right]Axy_{i,j} \quad \text{……..(19)}$$

Also, the fluxes of momentum in the x-direction into the (i,j)th cell across the face is equal to:

$$F(i,j)_x=\frac{1}{2}\left[\left(p+\rho u^2\right)_{i,j+1}+\left(p+\rho u^2\right)_{i,j}\right]Ayx_{i,j}-\frac{1}{2}\left[(\rho uv)_{i,j+1}+(\rho uv)_{i,j}\right]Axx_{i,j} \quad \text{……...(20)}$$

In the same way the fluxes of momentum across other faces can be written as follows:-

$$\frac{\Delta\overline{U}}{\Delta t}\times\Delta Vol=\overline{F}^{\,n+1} \quad \text{……..……..(21)}$$

where:

$$\Delta\overline{U}=\begin{vmatrix}\Delta\rho\\ \Delta(\rho u)\\ \Delta(\rho v)\end{vmatrix} \text{ and } \qquad \overline{F}^{\,n+1}=\begin{vmatrix}F^{n+1}\\ F_x^{\,n+1}\\ F_y^{\,n+1}\end{vmatrix}$$

……..(22)

The final equation can be re-written as follows:

$$\rho^{n+1}=\rho^n+\overline{F}^{\,n+1}\frac{\Delta ti}{\Delta Vol} \quad \text{……..……..(23)}$$

$$u^{n+1}=\frac{\left[(\rho u)^n+\overline{F}_x^{\,n+1}\dfrac{\Delta ti}{\Delta Vol}\right]}{\rho^{n+1}} \quad \text{……..……(24)}$$

$$v^{n+1}=\frac{\left[(\rho v)^n+\overline{F}_y^{\,n+1}\dfrac{\Delta ti}{\Delta Vol}\right]}{\rho^{n+1}} \quad \text{……..…..(25)}$$

Time Step

In general, for explicit methods, the value of Δt cannot be arbitrary, rather it must be less

than some maximum values for stability. The time dependent applications described above deal with governing flow equations that are hyperbolic with respect to time. Then, it is stated that Δt must obey the (CFL). The CFL criterion states that physically the explicit time step must be no greater than the time required for a sound wave to propagate from one grid to next. The maximum allowable value of CFL factor for stability in explicitly time dependent finite volume calculation can vary from approximately (0.5-1.0)[12]. On the other hand, the CFL is a function of fluid velocity and speed of sound and there is variation with the spatial coordinate, then the local value of Δt associated with each cell point will be different from one point to the next. Finally, the value of time step, which subjected to a stability criterion employed, should be minimum overall the cell points. To determine the value of time step, the following version of the CFL criterion is used. It is more practical to use the following simplified relation:

$$\frac{1}{\sqrt{\gamma}}(c+a)\frac{\Delta ti}{\Delta 1}\le 1 \quad \text{.....(26)}$$

Where, $a=\sqrt{\gamma\times R\times T}$ .....(27)

Damping Terms

Damping terms ensure stability, without it the convergence will not take place at all. Introducing damping in the partial differential equations therefore ensures numerical stability[12]. A non-derivative term is added to the governing equations, so the second order accuracy damping term for the velocity in x-direction can be written as follows[13]:

$$D_u(i,j)^{n+1}=\frac{B}{4}[u(i-1,j)+u(i+1,j)+]$$
$$u(i,j-1)+u(i,j+1)-4u(i,j) \quad \text{.....(28)}$$

where *B* is a damping factor generally less than one[13].

Relaxation Terms

The presence of the damping terms must not be allowed to contaminate the second order accuracy of the converged, time-steady solution, so a correction term $C\overline{F}$ is added at the explicit time level to ensure this,

$$C\overline{F}^{\,n}=(1-RF)\times C\overline{F}^{\,n-1}-RF\times\overline{D}^{\,n} \quad \text{.....(29)}$$

where, the relaxation term for the velocity in x-direction becomes:

$$CF_u(i,j)^n=(1-RF)\times CF_u(i,j)^{n-1}-RF\times D_u(i,j)^n$$

.....(30)

Now, the Equation (24) becomes:

$$u^{n+1}=\frac{\left[(\rho u)^n+\overline{F}_x^{\,n+1}\dfrac{\Delta ti}{\Delta Vo1}\right]}{\rho^{n+1}}+D_u^{n+1}+CF_u^{\,n}\cdots\cdots$$

.....(31)

With the same procedure the final equations for other properties can be written similar to form of Equation (31).

Results and Discussion

A finite volume method is employed to solve the equations of continuity, momentum and energy along a convergent-divergent diffuser. In this section, results of performance predicted in a convergent-divergent diffuser are presented. For each operating condition, there is a certain value of geometrical throat area corresponding to free-stream Mach number. This work is based on theoretical analysis only. But, the results of computational method is compared with analytical solution that based on oblique and normal shock relations (one dimensional flow) as shown in tables (1 through 3).

Figure (5) presents the Mach number distribution along a convergent-divergent diffuser length for different free-stream Mach number values. The value of each Mach number after normal shock starts to increase from the diffuser entrance position to the throat position (until reaching to choking condition at throat section). This is due to the subsonic expansion process across the convergent passage. Then it is starting to decrease along the divergent passage until reaching engine face position at a specified range (0.2-0.5)[13].

Figure (6) shows the static pressure distribution along the whole diffuser length for different free-stream Mach number. The value of pressure start to decreases along the convergent passage, and start to increases along the divergent passage until reaching engine face at acceptable range.

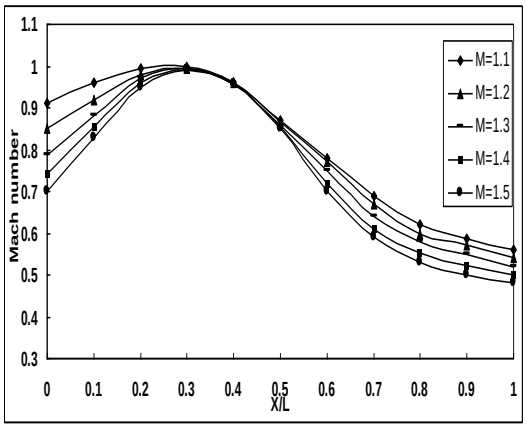

Fig. 5. Mach number distribution after normal shock (M_y) along convergent-divergent diffuser for different free-stream Mach numbers M_x=(1.1-1.5)

Fig. 6. Static pressure distribution along

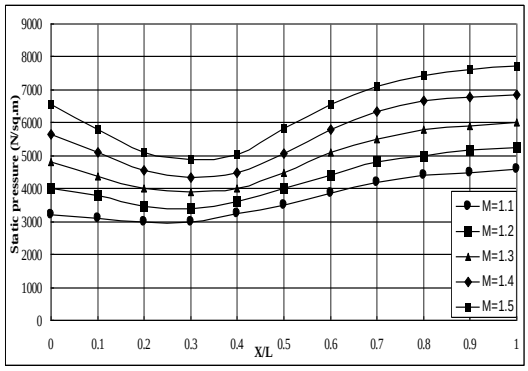

convergent-divergent diffuser for different free-stream Mach numbers M_x= (1.1-1.5)

Figures (7), (8), and (9) present the absolute velocity vector plot distribution along the supersonic air intake in off-design condition for Mach number 1.1,1.3 and 1.5 respectively. In all figures, the velocity distribution has high value behind the normal shock wave and continues to increase until reach to maximum value at diffuser throat, then it drops gradually to acceptable values at the engine face.

Figures (10), (11), and (12) present the contour lines of Mach number distribution along the supersonic air intake at off-design condition. The Mach number distribution has subsonic values behind the normal shock wave and it starts to increase along the converging passage until reaching maximum value at diffuser throat, (corresponding to choking mass flow rate at throat), then it drops gradually to acceptable values at the engine face.

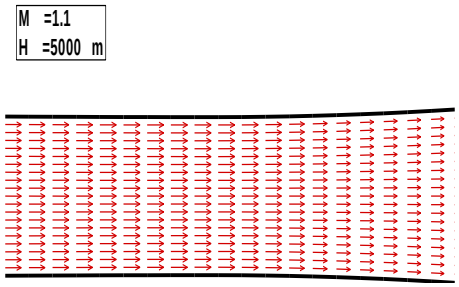

Fig. 7. Absolute velocity vector distribution along convergent-divergent diffuser (M=11)

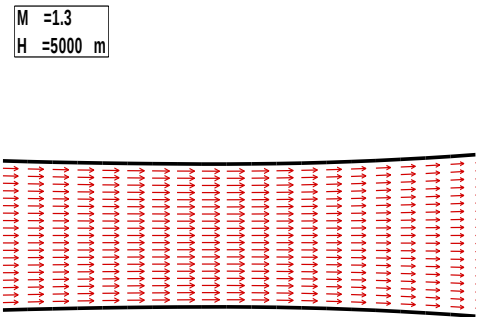

Fig. 8. Absolute velocity vector distribution along convergent-divergent diffuser (M=13)

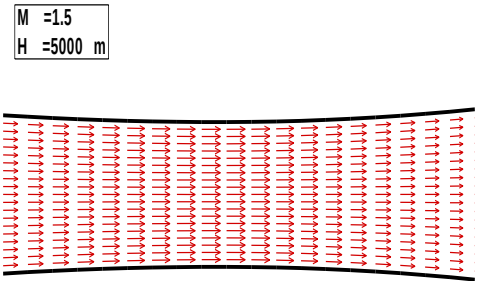

Fig. 9. Absolute velocity vector distribution along convergent-divergent diffuser (M=15)

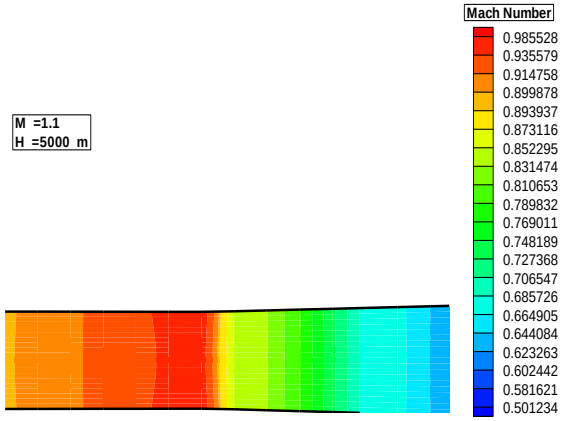

Fig. 10. Mach number contour line distribution along convergent-divergent diffuser (M=1.1)

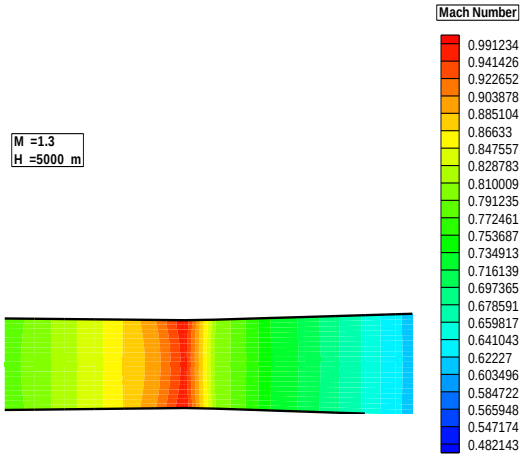

Fig. 11. Mach number contour line distribution along convergent-divergent diffuser (M=1.3)

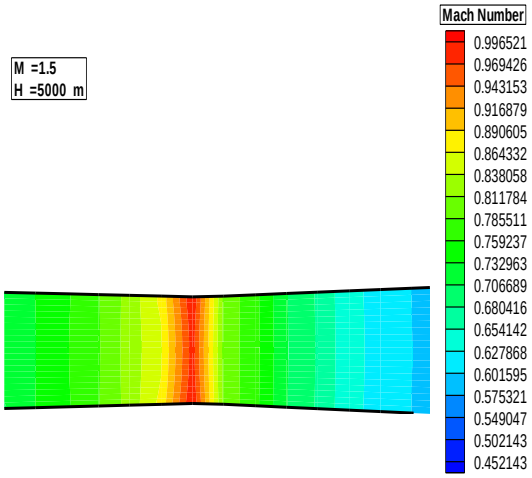

Fig. 12. Mach number contour line distribution along convergent-divergent diffuser (M=1.5)

Comparison of one dimensional flow with two dimensional flow results are done to show the accuracy of the time marching technique. The one dimensional flow was solved using normal shock wave relations and isentropic flow through the convergent-divergent diffuser.

The difference between one and two dimensional flow is due to neglected the velocity vector in y-direction (v) in one dimensional flow, and this difference in one and two dimensional flow can be observed in tables (1 through 3) as follows below.

Finally a computer program in Fortran-90 was built to solve the above governing equations.

Conclusions

This part of study is associated with numerical solution which operates at low supersonic Mach number ($M_\infty \leq 1.5$), where the normal shock wave stands at inlet cowl lip of the intake. The following conclusions can be drawn:-

1- Implementation of Time-Marching scheme has succeeded in the prediction of the choked flow region, which is important in the study of the performance of convergent-divergent diffuser.

2- Across the normal shock wave position, as the upstream shock Mach number (M_x) increases, the shock wave strength (effect) increases which cause to high loss in pressure recovery and decrease in downstream Mach number (M_y), and this situation may be causes increasing in the flow compression process along the convergent part.

3- The change in aircraft altitude has no effect on the shock wave position or strength, therefore, the height changes does not consideration in this paper.

4- The downstream shock wave Mach numbers (M_y) distribution along the convergent part of supersonic diffuser at different upstream Mach numbers (M_x) are increasing till reaching to maximum value at throat position (when flow is choking, $M_t = 1.0$), then it is starting to reduce along divergent part independently

on the values of free-stream Mach number (1.1-1.5) as shown in Figure 5.

5- The results from the finite volume method have been compared with analytical results from gas dynamics equations of one-dimensional flow, for the same diffuser geometry, and the agreement between them is good.

Geometry Data For Supersonic Air Intake

The performance prediction of supersonic air intake was made under design conditions. That means, the performance has been studied after design completion. The elements of convergent-divergent supersonic diffuser are (convergent diffuser capture height, convergent diffuser length, inlet cowl lip declination angle, divergent diffuser exit height, diffuser divergent angle, and divergent diffuser length). The geometry data for on-design is found equal to:-

L_c=110 cm, L_e=140 cm, θe=0.65 deg.

dc=46.7 cm, de=51.8 cm, δ =1.90 deg.

References

1- Conners, James F., and Meyer, C., “Design Criteria for Axisymmetric and Two-Dimensional Supersonic Inlets and Exits”, NACA TN 3589, 1956.

2- Knight, and Doyle, D., “Calculation of High-Speed Inlet Flows using the Navier-Stokes Equations”, Aircraft Journal, Vol.18, No.9, Sep.1981.

3- Shimabukuro, K.M., Welge, H.R., and Lee, A.C., “Inlet Design Studies for a Mach 2.2 Advanced Supersonic Cruise Vehicle”, Aircraft Journal, Vol.19, No.7, P.P. 367-369, July.1982.

4- Biringen, S., “Numerical Simulation of Two-Dimensional Inlet Flow Fields”, Aircraft Journal, Vol.21, No.4, P.P. 212-215, April 1984.

5- Walters, R.W., Douglas, L., and Hassan, H.A., “A Strong Implicit Procedure for the Compressible Navier-Stokes Equations”, AIAA Journal, Vol.24, No.1, P.P. 643-644, Jan. 1986.

6- Moretti, and Gino, “Efficient Euler Solver with Many Applications”, AIAA Journal, Vol.26, No.6, P.P. 755-757, June 1988.

7- Mittal, S., Jain, V., and Sullerey, R.K., “Numerical Investigation of Supersonic Mixed-Compression Inlet using Euler Equation”, NCABE Journal, Vol.14, No.6, Dec.2000.

8- Mattingly, J.D., Heiser, W.H., and Daley, D.H., “Aircraft Engine Design”, AIAA Education Series, Air Force Institute of Technology, Ohio, 1987.

9- Hill, P.G., and Peterson, C.R., “Mechanics and Thermodynamics of Propulsion”, Addison-Wesley Publishing Co., New Jersey, 1965.

10- Nicolai, L.M., “Fundamentals of Aircraft Design”, Addison-Wesley Publishing Co., Ohio, 1969.

11- Oosthuizen, P.H., and Carscallen, W.E., “Compressible Fluid Flow”, McGraw-Hill Book Co., 1997.

12- Farge, T.Z., “The Time Marching Method to Calculate Flow in Turbo machinery”, Msc. Thesis, University of Liverpool, Oct. 1985.

13- Charles, H., “Numerical Computation of Internal and External Flows”, Brussels, Belgium Univ., Publisher John Wiley & Sons Ltd. Vol.1, 1988.